JACS
JOURNAL OF THE AMERICAN CHEMICAL SOCIETY

Article

pubs.acs.org/JACS

Carbohydrate-Assisted Combustion Synthesis To Realize High-Performance Oxide Transistors

Binghao Wang,[†,‡] Li Zeng,[§] Wei Huang,[†] Ferdinand S. Melkonyan,[†] William C. Sheets,[∥] Lifeng Chi,[‡] Michael J. Bedzyk,*[,§] Tobin J. Marks,*[,†,§] and Antonio Facchetti*[,†,∥]

[†]Department of Chemistry and the Materials Research Center, Northwestern University, 2145 Sheridan Road, Evanston, Illinois 60208, United States

[‡]Institute of Functional Nano & Soft Materials (FUNSOM), Jiangsu Key Laboratory for Carbon-Based Functional Materials and Devices, Soochow University, 199 Ren'ai Road, Suzhou 215123, China

[§]Applied Physics Program, Materials Science and Engineering Department and the Materials Research Center, Northwestern University, 2220 Campus Drive, Evanston, Illinois 60208, United States

[∥]Polyera Corporation, 8045 Lamon Avenue, Skokie, Illinois 60077, United States

Supporting Information

ABSTRACT: Owing to high carrier mobilities, good environmental/thermal stability, excellent optical transparency, and compatibility with solution processing, thin-film transistors (TFTs) based on amorphous metal oxide semiconductors (AOSs) are promising alternatives to those based on amorphous silicon (a-Si:H) and low-temperature (<600 °C) poly-silicon (LTPS). However, solution-processed display-relevant indium-gallium-tin-oxide (IGZO) TFTs suffer from low carrier mobilities and/or inferior bias-stress stability versus their sputtered counterparts. Here we report that three types of environmentally benign carbohydrates (sorbitol, sucrose, and glucose) serve as especially efficient fuels for IGZO film combustion synthesis to yield high-performance TFTs. The results indicate that these carbohydrates assist the combustion process by lowering the ignition threshold temperature and, for optimal stoichiometries, enhancing the reaction enthalpy. IGZO TFT mobilities are increased to >8 $cm^2\ V^{-1}\ s^{-1}$ on SiO_2/Si gate dielectrics with significantly improved bias-stress stability. The first correlations between precursor combustion enthalpy and a-MO densification/charge transport are established.

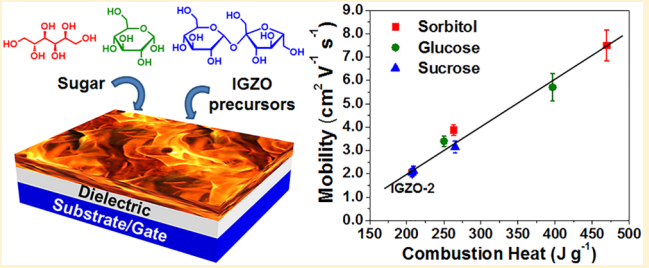

INTRODUCTION

Flat panel displays encompass a growing number of electronic visual technologies and are far lighter, thinner, and of higher resolution than conventional designs.[1−3] Although amorphous silicon (a-Si:H) is typically used in thin-film switching transistors (TFTs) for active-matrix liquid crystal displays (AMLCDs) or active-matrix organic light-emitting diode displays (AMOLEDs),[4−8] it is limited by low field-effect mobility (~0.5−1.0 $cm^2\ V^{-1}\ s^{-1}$) and poor current-carrying properties.[9−12] Thus, low-temperature (≤600 °C) poly-silicon (LTPS) TFTs fabricated on glass substrates, with mobility >50 $cm^2\ V^{-1}\ s^{-1}$ and good current-carrying properties, are attractive for next-generation display technologies.[13−15] However, LTPS TFT production is capital- and energy-intensive, and the resulting TFTs exhibit poor electrical uniformity and high off-current levels.[16−18] Significant research carried out on amorphous metal oxide semiconductors (AOSs) has demonstrated that they are promising alternatives to LTPS.[19−22] Due to their outstanding electrical properties, excellent optical transparency, and remarkable mechanical flexibility, a-MO TFTs with mobilities of ~5−10 $cm^2\ V^{-1}\ s^{-1}$, achieved by sputtering indium-gallium-zinc oxide (IGZO) films, have reached large-scale manufacture.[23−25] More recently, with the aims of lowering processing temperatures, reducing production costs, and enabling high-throughput deposition by printing on plastic substrates, solution-processed a-MO TFTs, and particularly those based on IGZO, have advanced significantly.[26−30] In pioneering studies, solution-processed IGZO TFTs were realized at 150−250 °C using deep-UV irradiation, sol−gel on a chip, spray pyrolysis, high-pressure thermal annealing, and combustion synthesis.[31−34] However, the saturation mobilities of these devices on low-capacitance SiO_2 dielectrics remain modest (~1−3 $cm^2\ V^{-1}\ s^{-1}$), with generally inferior bias-stress stability (5−10 V threshold voltage shift) versus state-of-the art sputtered IGZO TFTs. This likely reflects high defect densities and incomplete lattice densification.

In this laboratory, we have explored the use of combustion synthesis for fabricating thin-film a-MO electronics, including semiconductors, contacts, and more recently gate dielectrics,[35,36] and several other laboratories have validated this

Received: March 7, 2016
Published: May 11, 2016

DOI: 10.1021/jacs.6b02309
J. Am. Chem. Soc. 2016, 138, 7067−7074

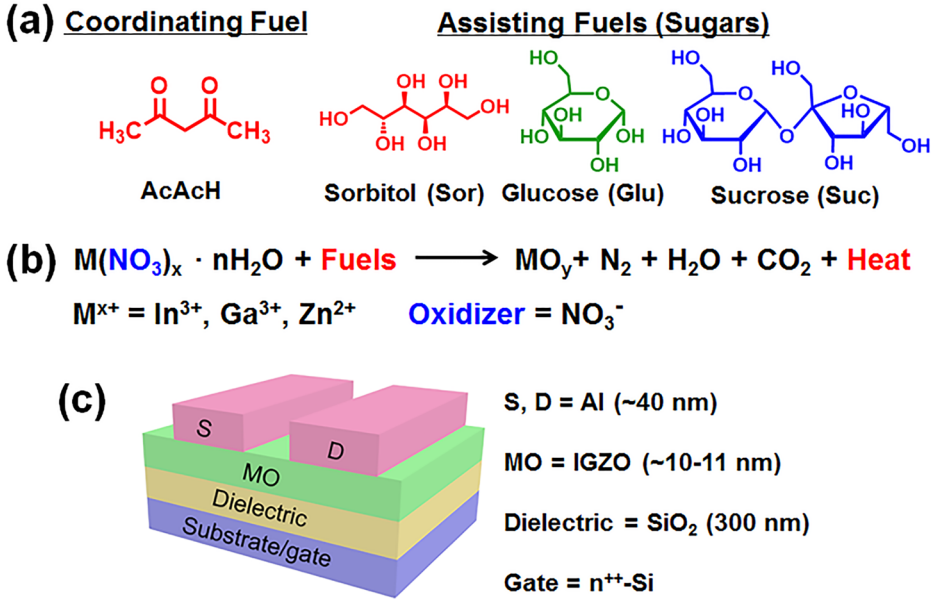

Figure 1. (a) Chemical structures of acetylacetone and of sorbitol, β-glucose, and sucrose implemented as fuels in oxide combustion synthesis. (b) Schematic of the combustion synthesis chemical reaction. Note that all species in the reaction have not been identified; this schematic shows an idealized reaction. (c) Top-contact, bottom-gate MO TFT structure used here.

strategy.[37−41] By employing exothermic oxidant and fuel reactions, the self-generated and localized energy converts metal precursors into the corresponding a-MOs at low input temperatures.[34] Note, however, that only a single fuel, acetylacetone (AcAcH), which also acts as a ligand for the metal constituents, was explored in depth in combination with metal nitrates. From these studies it was established that, although combustion can occur at temperatures as low as 150 °C, the MO precursors typically require some degree of pre-decomposition before vigorous autocatalytic combustion initiates.[42] Thus, small quantities of reactants cannot generate the critical amounts of the pre-decomposed species necessary for ignition. For very thin films, the loss of autocatalytic species due to high surface-to-volume ratios can suppress rapid combustion and result in inefficient precursor → MO product conversion. Therefore, minimum thin-film combustion temperatures to achieve respectable TFTs are >200 °C: i.e., ∼200 °C for In_2O_3 ($\mu \approx 0.61$ cm^2 V^{-1} s^{-1}),[43] ∼225 °C for ZTO ($\mu \approx 0.29$ cm^2 V^{-1} s^{-1}) and IZO ($\mu \approx 0.32$ cm^2 V^{-1} s^{-1}),[33] and ∼250 °C for IYO ($\mu \approx 0.75$ cm^2 V^{-1} s^{-1})[44] and IGZO ($\mu \approx 0.77-1.28$ cm^2 V^{-1} s^{-1}), depending on metal composition.[34,35] Note that, for display-relevant IGZO TFTs and combustion temperatures of 300 °C, the average electron mobilities remain ∼3 cm^2 V^{-1} s^{-1} for Si/SiO_2 gate dielectrics.[33,34,42,44]

These results raise the intriguing question as to whether fuels that are more effective/exothermic than AcAcH are possible[45] and whether they can be environmentally benign to address sustainability issues in semiconductor processing.[46] In this contribution we report that simple sugars are remarkably effective fuels for the combustion synthesis of IGZO thin films and afford significantly enhanced TFT performance. Note that these nontoxic chemicals are used as propellants in "rocket candy", mixtures of sugar fuel and KNO_3 oxidizer.[47,48] Our results indicate that these carbohydrates assist the combustion processes by depressing the ignition temperatures and, for optimal stoichiometries, enhance the measured enthalpy of reaction. Consequently, IGZO TFT mobilities increase to >8 cm^2 V^{-1} s^{-1} with significantly reduced bias-stress shifts. For the first time, clear correlations between precursor combustion enthalpy and a-MO densification/charge transport are established.

EXPERIMENTAL SECTION

Combustion Precursor Preparation. All combustion precursor materials were purchased from Sigma-Aldrich and stored in a vacuum desiccator. For IGZO TFT precursors, appropriate amounts of the metal salts $In(NO_3)_3$, $Zn(NO_3)_2$, and $Ga(NO_3)_3$, molar ratio 1:0.11:029, were dissolved in 2-methoxyethanol to achieve a 0.05 M metal concentration. Acetylacetone and ammonium hydroxide solutions (28% NH_3 in H_2O) were then added, and the mixture was allowed to stir overnight. The M^{n+}:AcAcH molar ratios were 1:2 (IGZO-1), 1:4 (IGZO-2), and 1:6 (IGZO-3). The AcAcH:NH_4OH volumetric ratio was 2:1. Three sugars were separately dissolved in deionized water to achieve 40 mg mL^{-1} solutions and stirred overnight. An appropriate amount of sugar solution to achieve 5, 10, 15, or 20 wt% sugar vs the total metal weight was next added to the metal solution. The resulting x wt% sugar/IGZO-n solution was stirred for 1 h before spin-coating.

DSC and TGA Measurements. These measurements were performed on an SDT Q600 (TA Instruments Inc.) instrument under N_2. Experiments were carried out on 2−3 mg samples of precursor powders that were dried under vacuum (Schlenk line). The heating rate was 10 °C min^{-1} under a 70 mL min^{-1} N_2 flow.

Thin-Film Fabrication and Electrical Characterization. All solutions were filtered through 0.2 μm syringe filters before fabrication. n^{++} silicon wafers with 300 nm SiO_2 (WRS Materials) used as substrates were solvent-cleaned and then cleaned with an O_2 plasma for 5 min before use. IGZO precursors were spin-coated on silicon wafers at 3500 rpm for 30 s and subsequently annealed for 20 min at 300 °C for each layer in ambient (relative humidity ∼30%). This process was repeated another three times to obtain the desired film thickness. Al source and drain (S/D) electrodes (thickness = 40 nm) were deposited by thermal evaporation through a metal shadow mask. The channel width and length for all devices were 1000 and 100 μm, respectively. TFT characterization was performed under ambient conditions using an Agilent 4155C semiconductor parameter analyzer. The carrier mobility (μ) was evaluated in the saturation region with the conventional metal−oxide−semiconductor field-effect transistor model using eq 1,[49−51]

DOI: 10.1021/jacs.6b02309
J. Am. Chem. Soc. 2016, 138, 7067−7074

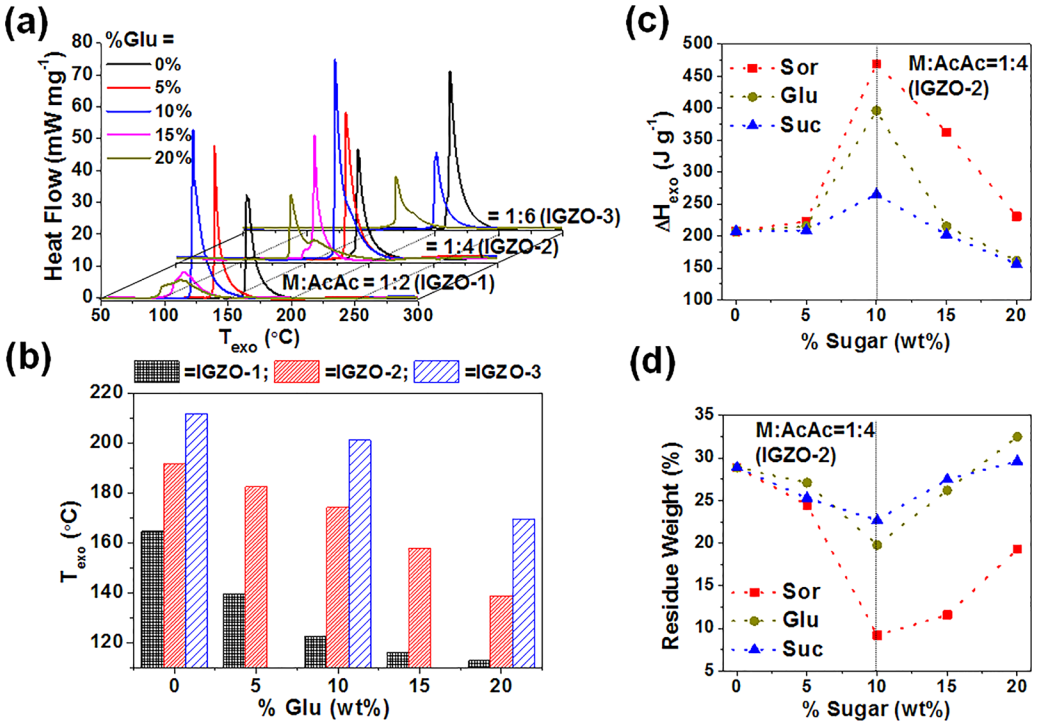

Figure 2. (a) DSC plots for IGZO-1 (M:AcAcH = 1:2), IGZO-2 (M:AcAcH = 1:4), and IGZO-3 (M:AcAcH = 1:6) dry precursors with differing glucose contents. (b) DSC-derived peak exotherm temperatures for IGZO-1, IGZO-2, and IGZO-3 precursors. (c) Combustion enthalpy for IGZO-2 precursors with different carbohydrate fuel contents (Sor, Glu, Suc) during the combustion process. (d) TGA-derived residual weights at 300 °C for IGZO-2 precursors with differing sugar contents.

$$I_{DS} = \frac{\mu C_i W}{2L}(V_{GS} - V_T)^2 \quad (1)$$

where I_{DS} is the drain-source current, C_i is the dielectric capacitance per unit area (the C_i of 300 nm SiO_2 is 11 nF cm^{-2} without frequency dependence), W and L are the channel width and length, respectively, V_{GS} is the gate-source voltage, and V_T is the threshold voltage.

Oxide Film Structural Characterization. Surface roughness was measured with a Bruker Dimensional Icon atomic force microscopy (AFM) system in the tapping mode. Grazing incidence X-ray diffraction (GIXRD) data were acquired with a Rigaku Smartlab thin-film diffraction workstation using Cu Kα (1.54 Å) radiation. X-ray photoelectron spectroscopy (XPS) was performed on a Thermo Scientific ESCALAB 250 Xi spectrometer. X-ray absorption fine structure (XAFS) measurements were conducted at sector 5BMD at the Advanced Photon Source at Argonne National Laboratory. The incident beam energies were tuned to near the In K-edge (27.940 keV), films on quartz glass were placed from the incident direction, and data were collected in fluorescence mode using two four-element silicon drift detectors (SII NanoTechnology). The normalized linear EXAFS absorption coefficient $\chi(k)$ can be fit by eq 2,

$$\chi(k) = \sum_i \frac{N_i(\theta)|f_i(k)|S_0^2}{kR_i^2} \sin[2R_i k + \phi_i(k)]\, e^{-2R_i/\lambda(k)}\, e^{-2\sigma_i^2 k^2} \quad (2)$$

where S_0^2 is the intrinsic loss factor, $e^{-2R_i/\lambda(k)}$ is the attenuation factor related to the electron mean free path $\lambda(k)$, N_i and R_i are the coordination number and bond distance of the ith shell of the absorbing atom, respectively, $f_i(k)$ and $\phi_i(k)$ are the back-scattering amplitude and the phase shift, respectively, and $e^{-2\sigma_i^2 k^2}$ is the Debye–Waller factor—a measure of the structural disorder or the variation in R_i. The Fourier transform of $\chi(k)$ can generate a *pseudo*-radial distribution function (p-RDF) for the absorbing atom. Film thickness was measured by using a spectroscopic ellipsometer (J.A. Woollam, ESM-300). To ensure accuracy, the thickness of SiO_2 for each Si/SiO_2 substrate was measured before film deposition, and the same fitting parameters were used for all the films.

RESULTS AND DISCUSSION

Glucose-Assisted Transistor Measurements. Figure 1 shows the chemical structures of AcAcH, the carbohydrates used in this study, and a schematic of the combustion synthesis reaction. Note that here we investigate metal oxide compositions comprising Ga as an O "getter", which enables a better control of the carrier density. However, IGZO requires higher temperatures to achieve full densification and stable (hysteresis- and bias-stress-free) TFT performance. That is why the combustion temperatures explored here are higher than in our previous investigations.[33] In preliminary IGZO TFT measurements (details in Supporting Information (SI), Figures S1–S3 and Table S1), glucose was used to identify the optimal metal (In+Ga+Zn):AcAcH molar ratio (M:AcAcH) as well as the effect of the glucose content in the combustion formulation, expressed as weight percentage vs the total metal weight (wt% Glu), on the TFT metrics. In these experiments, M:AcAcH = 1:2 (identified as composition IGZO-1), 1:4 (IGZO-2), and 1:6 (IGZO-3) plus x wt% Glu = 0, 5, 10, 15, 20% precursor formulations (indicated here as x wt% Glu/IGZO-n, n = 1–3) were screened. The precursor formulations comprising the metal source (nitrates), AcAcH, glucose (or other sugars, *vide infra*), and a base (28% NH_3 in H_2O) in 2-methoxyethanol were spin-coated on 300 nm Si/SiO_2 substrates, and the resulting films thermally processed at 300 °C for 20 min. This process was repeated another three times to achieve the desired IGZO film thicknesses of ~10–11 nm. Finally, 40 nm thick Al source and drain electrodes were deposited through a shadow mask. The channel length and width for all devices are 100 and 1000 μm, respectively.

DOI: 10.1021/jacs.6b02309
J. Am. Chem. Soc. 2016, 138, 7067–7074

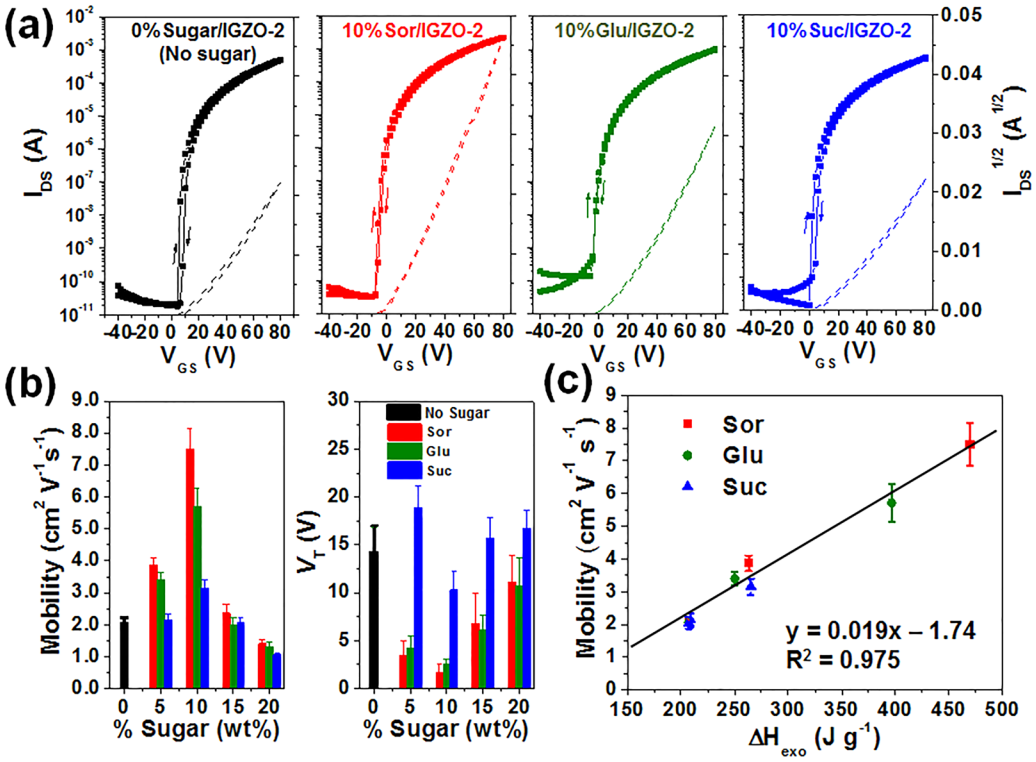

Figure 3. (a) Transfer characteristics for no sugar addition and 10 wt% sugars/IGZO-2 TFTs for the indicated sugars. (b) Mobility and threshold voltage (V_T) statistics for x wt% sugar/IGZO-2 TFTs, with the indicated sugar composition. (c) Linear correlation between carrier mobility and enthalpy of combustion for x wt% sugar ≤10, with the indicated sugar composition.

The present TFT data indicate that the IGZO field-effect electron mobility (μ) depends on the glucose content and maximizes at wt% Glu = 10 for all M:AcAcH ratios (Figure S3). Thus, the maximum mobility for 10 wt% Glu/IGZO-1 is significantly lower (3.92 $cm^2 V^{-1} s^{-1}$) than that of 10 wt% Glu/IGZO-2 (6.51 $cm^2 V^{-1} s^{-1}$), although the μ of the IGZO-1 (2.7 $cm^2 V^{-1} s^{-1}$) is larger than that of IGZO-2 (2.1 $cm^2 V^{-1} s^{-1}$). For all x wt% Glu/IGZO-3 devices, the mobility variation with the glucose content is small ($\mu \approx 1.5-1.9$ $cm^2 V^{-1} s^{-1}$), and the largest mobility achieved for 10 wt% Glu is far lower than those achieved for IGZO-1 and IGZO-2 TFTs at the same Glu content. As assessed by AFM images, the latter result reflects poor film morphology for all %Glu/IGZO-3 compositions (see Figure S4), where high-porosity film microstructures increasingly dominate as the glucose content increases. Such morphologies are doubtless detrimental to mobility. Furthermore, note that the electron mobilities of IGZO TFTs fabricated with added glucose in the formulation but without AcAcH exhibit poor performance (μ = 0.6–2.0 $cm^2 V^{-1} s^{-1}$), which decreases monotonically with increasing wt% Glu (see Table S2). These initial results indicate that AcAcH is necessary for efficient glucose fuel combustion, with the sugar acting as an assisting/supporting fuel whereas coordinating ligand AcAcH is the primary fuel. This result parallels the lower acidity of glucose hydroxyl groups (−OH, $pK_a \approx 14$) versus that of AcAcH ($pK_a \approx 9$),[S2,S3] thereby preventing efficient metal ion coordination in the competing presence of the base (NH_4OH) in the IGZO precursor formulation. Furthermore, a near-stoichiometric amount of AcAcH vs total metals (M:AcAcH = 1:4) and wt% Glu = 10 affords the best-performing IGZO transistors.

Thermal Analysis. To understand the x wt% Glu/IGZO-n device performance variations before exploring related carbohydrates, the thermal evolution of the combustion process was characterized by differential scanning calorimetry (DSC) and thermogravimetric analysis (TGA). Figure 2 shows DSC plots for various precursor compositions from which the peak exotherm temperature (T_{exo}) and enthalpy of combustion (ΔH_{exo}) can be extracted. From these measurements note that both T_{exo} and ΔH_{exo} are strongly dependent on the wt% Glu and that the thermal analysis data correlate with the IGZO TFT performance. Interestingly, for all dry precursors (see Experimental Section for details), the combustion temperature T_{exo} decreases as M:AcAcH falls and, equally relevant, as wt% Glu increases. Thus, at constant temperature ramp rate, T_{exo} for M:AcAcH = 1:2 (IGZO-1), 1:4 (IGZO-2), 1:6 (IGZO-3) declines from 164.5, 191.6, and 211.7 °C, respectively, for the sample without glucose to 122.6, 174.1, and 201.0 °C, respectively, for 10 wt% Glu and to 112.8, 138.7, and 169.4 °C, respectively, for 20 wt% Glu. However, ΔH_{exo} has a very different behavior, with the combustion enthalpy increasing dramatically from 174.1 (M:AcAcH = 1:2) and 207.2 J g^{-1} (M:AcAcH = 1:4) for wt% Glu = 0, to 314.8 (M:AcAcH = 1:2) and 396.5 J g^{-1} (M:AcAcH = 1:4) for wt% Glu = 10, respectively, and then decreasing to 161–165 (M:AcAcH = 1:2) and 161–186 J g^{-1} (M:AcAcH = 1:4) for larger glucose contents (wt% Glu = 15–20). For M:AcAcH = 1:6, the ΔH_{exo} decreases from 356.4 to 221.7 J g^{-1} for 10 wt% Glu and then to 184.5 J g^{-1} for 20 wt% Glu. Note that, unlike the high combustion efficiency of melt-mixed sugars + nitrates,[54] solid glucose + In/Ga/Zn nitrate IGZO precursor formulations without AcAcH do not exhibit any significant exotherms (DSC in Figure S5 and Video S1) nor abrupt mass loss (see TGA in Figure S6), consistent with the poor electron mobilities measured for the corresponding IGZO films. These results indicate that sugar addition to combustion synthesis fuels

DOI: 10.1021/jacs.6b02309
J. Am. Chem. Soc. 2016, 138, 7067–7074

Table 1. Performance Metrics of Sugar-Assisted Combustion-Synthesized IGZO TFTs on 300 nm Si/SiO_2 Substrates with Al Source-Drain Electrodes[a]

semiconductor	mobility ($cm^2 V^{-1} s^{-1}$)	V_T (V)	V_{ON} (V)	I_{on}/I_{off}
0% sugar/IGZO-2	2.05 ± 0.18	14.3 ± 2.6	3.9 ± 1.8	~10^7
5% Sor/IGZO-2	3.87 ± 0.23	3.5 ± 1.5	−5.7 ± 2.5	~10^6
10% Sor/IGZO-2	7.50 ± 0.66	1.7 ± 0.9	−8.2 ± 3.8	~10^5−10^7
15% Sor/IGZO-2	2.36 ± 0.28	6.8 ± 3.2	−3.3 ± 1.6	~10^7
20% Sor/IGZO-2	1.42 ± 0.11	11.1 ± 2.8	0.1 ± 2.2	~10^7
5% Glu/IGZO-2	3.40 ± 0.22	4.2 ± 1.3	−4.3 ± 2.1	~10^6
10% Glu/IGZO-2	5.71 ± 0.58	2.5 ± 0.6	−11.5 ± 3.6	~10^5−10^7
15% Glu/IGZO-2	2.01 ± 0.21	6.1 ± 1.5	−5.7 ± 2.7	~10^7
20% Glu/IGZO-2	1.30 ± 0.16	10.7 ± 3.0	1.1 ± 2.8	~10^7
5% Suc/IGZO-2	2.14 ± 0.19	18.9 ± 2.3	4.0 ± 2.6	~10^7
10% Suc/IGZO-2	3.15 ± 0.25	10.3 ± 1.9	0.3 ± 1.9	~10^7
15% Suc/IGZO-2	2.05 ± 0.16	15.7 ± 2.2	−0.9 ± 2.5	~10^7
20%Suc/IGZO-2	1.06 ± 0.07	16.7 ± 1.9	−1.5 ± 2.8	~10^7

[a]Average from ≥20 devices.

strongly affects the IGZO ignition temperatures, and a proper balance between metal content and coordinating fuel (AcAcH)/supporting fuel (sugar) significantly enhances the enthalpy of the metal oxide combustion synthesis and enhances the charge transport characteristics of the resulting TFTs.

The thermal properties of IGZO precursor compositions comprising IGZO-2 (M:AcAcH = 1:4) with two additional sugars, sorbitol and sucrose, were next investigated prior to TFT fabrication. Relevant DSC and TGA plots can be found in Figure S7, while the corresponding T_{exo}, ΔH_{exo}, and % residual weight (RW) at 300 °C as a function of the sugar content are shown in Figures 2c,d and S8. From the combined data the following conclusions can be drawn: (1) All sugars strongly depress T_{exo}, which falls for Sor, Glu, and Suc from 191.6 °C (wt% sugar = 0) to 169.4, 174.1, 173.5 °C (wt% sugar = 10) and to 136.5, 138.7, and 137.6 °C (wt% sugar = 20), respectively. (2) As in conventional combustion synthesis, T_{exo} corresponds to the temperature in the TGA where substantial weight loss occurs, indicating temporally abrupt formation of large quantities of gaseous products. (3) The combustion enthalpy, ΔH_{exo}, strongly depends on the sugar identity and follows the same dependence on wt% sugar as observed for glucose. Thus, remarkable ΔH_{exo} values of 469.5, 396.5, and 265.2 J g^{-1} are measured for Sor, Glu, and Suc, respectively, at wt% sugar = 10. Video S1 visualizes the exotherm differences for selected compositions. (4) While there is little, if any, correlation between T_{exo} and ΔH_{exo}, strong correlations are observed between ΔH_{exo} and RW for all sugars, where a greater ΔH_{exo} corresponds lower RW after combustion. Thus, since ΔH_{exo} maximizes for all sugars at ~10 wt%, RW is found to fall from ~25% (Suc) to 18% (Glu) and to 8% (Sor). These data demonstrate that sorbitol affords the cleanest IGZO film combustion process and that IGZO TFT performance should depend strongly on the sugar type and weight content.

TFT Performance Comparisons and Enthalpy−Transport Correlations. Next, IGZO TFTs were fabricated for IGZO-2 (M:AcAcH = 1:4) with other carbohydrates to define transport characteristics. Figures 3a, S1, and S9 show representative transfer plots, and Table 1 summarizes relevant parameters. Plots of the carrier mobility (left) and threshold voltage (right) for various x wt% sugar/IGZO-2 TFTs are shown in Figure 3b. For all carbohydrates, TFT carrier mobility follows a similar trend with sugar content, where μ first increases from ~2.0 (wt% sugar = 0) to 2.5−4.0 $cm^2 V^{-1} s^{-1}$ (wt% sugar = 5), maximizes for wt% sugar = 10 (8.2 $cm^2 V^{-1} s^{-1}$ for Sor, 6.5 $cm^2 V^{-1} s^{-1}$ for Glu, and 3.5 $cm^2 V^{-1} s^{-1}$ for Suc), and then falls to 2.0−3.5 (wt% sugar = 15) and ~1 $cm^2 V^{-1} s^{-1}$ (wt% sugar = 20) for larger sugar contents. Note that similar trends for mobility are expected for smaller channel length devices due to the small channel dependence of a-IGZO TFTs.[55] Also, lower operation voltages and higher electron mobilities could be achieved by using high-capacitance gate dielectrics, as widely shown in the literature.[34−36] Threshold voltage dependencies on sugar content vary, with V_T for Suc/IGZO-2 TFTs remaining large and within the same range (~10−20 V), whereas those of Sor/IGZO-2 and Glu/IGZO-2 TFTs first decrease from 14.3 (wt% sugar = 0) to ~3.5−4 V (wt% sugar = 5), reach a minimum at ~1.5−2.0 V for wt% sugar = 10, and then increase (~7−11 V) for larger amounts of sugar. In terms of turn-on voltage (V_{on}), sugar addition shifts V_{on} toward negative values, indicating a substantial reduction of deep traps.[35] Furthermore, all IGZO TFTs exhibit I_{on}/I_{off} in the range of 10^5−10^7, which are large considering that these devices do not have precisely patterned gate or semiconducting layers. Finally, the present sorbitol- or glucose-assisted IGZO devices exhibit minimal $I-V$ hysteresis, ~0.5 V for wt% sugar = 10 versus a far larger 4.0 V for 0 wt% sugar/IGZO-2. These exceptional data reflect a dramatically intensified combustion process and dense M-O-M lattice formation (*vide infra*). Interestingly, a clear correlation is established, independent of the sugar, between μ and ΔH_{exo}, and, excluding compositions having excess sugar, which likely contain carbonaceous impurities, the correlation is linear, with $R^2 \approx 0.98$ (Figure 3c).[56]

Next, positive-gate bias-stress evaluations were performed to compare IGZO-2 TFT operational stability with that of the high-mobility 10 wt% sugar/IGZO-2 TFTs (Figure S10). Devices were subjected to a V_{GS} constant bias of +20 V for 200 s intervals for 1200 s durations in ambient, without encapsulation or back channel protection. Figure S11 compares the normalized threshold voltage (ΔV_T) and mobility change versus bias time. The IGZO-2 device exhibits marked bias-related ΔV_T shifts (>+15 V), especially in the initial 200 s, implying a large density of acceptor-like electron-trapping states.[57] However, for the sugar-assisted IGZO-2 devices, the shifts are far smaller, especially for 10 wt% Sor/IGZO-2 ($\Delta V_T \approx +4.5$ V) and 10 wt% Glu/IGZO-2 ($\Delta V_T \approx +5.2$ V) TFTs. In terms of mobility retention, the 10 wt% Sor/IGZO-2 TFT

DOI: 10.1021/jacs.6b02309
J. Am. Chem. Soc. 2016, 138, 7067−7074

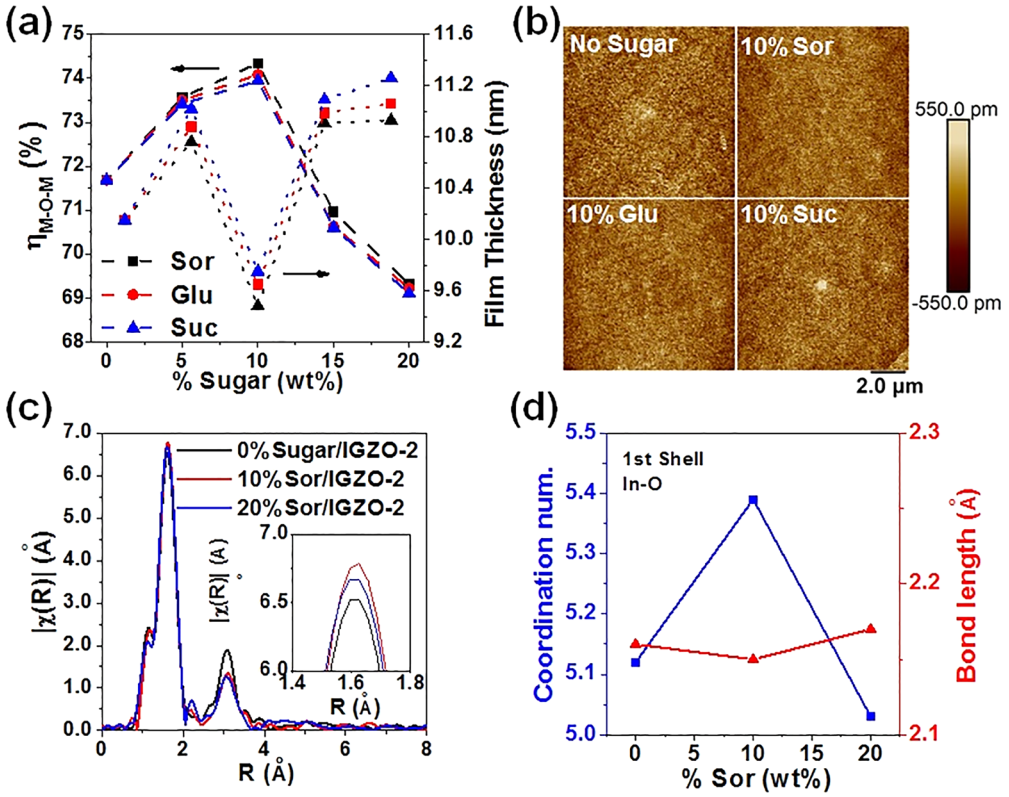

Figure 4. (a) Ratio of XPS O1s M-O-M peak area to total peak area and film thickness, plotted as a function of the indicated sugar concentration. (b) AFM images of IGZO-2 and 10% sugar/IGZO-2 films. (c) Comparison of the In K-edge *p*-RDFs of the IGZO, 10 wt% Sor/IGZO-2, and 20 wt % Sor/IGZO-2 films. (d) EXAFS-derived coordination numbers and In−O bond lengths for the indicated films.

exhibits a mobility nearly the same as the initial value, and the 10 wt% Glu/IGZO-2 TFT shows only a 3% fall in mobility. In contrast, the IGZO-2 device performs the most poorly, with a mobility fall of ∼90% versus the pre-bias value.

Thin-Film Morphology and Microstructure. To better understand the origin of the impressive sugar-assisted TFT performance, XPS measurements were performed. The intensity and type of O1s binding energy features is a good predicator of electron transport characteristics, since weakly bound O and/or O incompletely coordinated by metal ions can introduce trap states, reduce mobility, and enhance bias-stress instability in metal oxide TFTs.[58] The O1s peaks were deconvoluted into peaks for lattice M-O-M, M-OH, and weakly bound M-O-R (Figure S12).[56] The M-O-M peak area-to-total O1s peak area ratio (η_{M-O-M}, Figure 4a) indexes the film O lattice fraction and is known to correlate with oxide TFT performance.[26] The η_{M-O-M} is found to be a function of the precursor sugar concentration and, for all sugars, first increases with increasing the sugar content and then reaches a maximum at wt% sugar = 10. If highly exothermic combustion does not occur, incorporating large amounts of sugar (>10 wt%) decreases the M-O-M lattice content, probably because part of the oxidizing equivalents are consumed by excess sugar decomposition rather than in H_2O elimination/lattice densification. Note that accurate IGZO film thickness analysis by spectroscopic ellipsometry (see Experimental Section for details) supports this model. When highly exothermic combustion occurs for wt% sugar = 10, a significant film thickness contraction of ∼10% is detected. Note also that AFM images (Figure 4b) indicate that all films are very smooth, with σ_{RMS} ≈ 0.2 nm and without obvious cracking or porosity.

Finally, more detailed microstructural changes within the amorphous films were analyzed by EXAFS techniques to extract coordination numbers (N_i), bond lengths (R_i), and Debye−Waller (DW) factors for the atoms of interest.[59,60] Since sorbitol induces the most significant effects on IGZO TFT performance, the local structures of spin-coated 0 wt% sugar/IGZO-2 (control), 10 wt% Sor/IGZO-2 (optimal sample with sugar), and 20 wt% Sor/IGZO-2 (unoptimal sample with excess sugar) films were analyzed to probe structural−electrical performance correlations. Note that GIXRD data for the present IGZO films (Figure S13) confirm that all are amorphous. Due to the lower atomic concentrations of Ga and Zn in these IGZO films, only In K-edge spectra at 27.92 keV were analyzed. Figure 4c,d and Table S3 compare the *p*-RDFs (the Fourier transform for *k* range 1.13−11 $Å^{-1}$ with *k*-weight 2) and fitting results (two-shell model and fitting range of *R* = 1−3.5 Å) for three films. The peak intensities in the *p*-RDFs correlate with the N_i and *DW* factors of a particular shell, and higher peak intensities typically correspond to larger N_i values. The detailed extracted values for the first two shells are shown in Table S3. Cleary, the N_i value of 10% Sor/IGZO-2 (5.39) is higher than those of IGZO-2 without sugar (5.12) and 20% Sor/IGZO-2 (5.03), demonstrating that appropriate amounts of sugar enhance the density of the metal oxide nanostructure. For the second In-M (M = In, Ga, and Zn) shell, the peak intensities for all films were much lower than that of the first In-O shell, consistent with disordering of the polyhedral network (interconnectivity) and amorphous features.[58] In terms of the bond lengths, the calculated R_i values are relatively constant at ∼2.16 Å for the In-O shell and ∼3.35

DOI: 10.1021/jacs.6b02309
J. Am. Chem. Soc. 2016, 138, 7067−7074

Å for the In-M shell, comparable to the corresponding radii for sputtered IGZO films.[59]

CONCLUSIONS

This work demonstrates that simple, chemically innocuous carbohydrates serve as effective precursor fuel components in combustion processes for fabricating high-performance thin-film IGZO electronics. The unique self-generating energy characteristics significantly enhance carrier mobility and operational stability of the product TFTs, with clear correlations between the enthalpy of combustion, microstructural densification, M-O-M lattice content, and IGZO electron mobility. This process should be extendable to a broad range of metal oxides beyond those that are of immediate interest in TFT display applications, and should also applicable to other natural sugars and polysaccharides, such as xylitol, mannitol, and maltitol to cite just a few.

ASSOCIATED CONTENT

Supporting Information

The Supporting Information is available free of charge on the ACS Publications website at DOI: 10.1021/jacs.6b02309.

DSC and TGA curves of oxide precursors with/without coordinating fuel, AFM images and XPS data of IGZO films, output curves, and bias-stress test of IGZO TFTs, including Figures S1−S13 and Tables S1−S3 (PDF)

Video S1 (MOV)

AUTHOR INFORMATION

Corresponding Authors

*bedzyk@northwestern.edu

*t-marks@northwestern.edu

*a-facchetti@northwestern.edu

Notes

The authors declare no competing financial interest.

ACKNOWLEDGMENTS

We thank ONR (MURI N00014-11-1-0690), the Northwestern U. MRSEC (NSF DMR-1121262), AFOSR (FA9550-08-1-0331), and Polyera Corp. for support of this research. This work made use of the J. B. Cohen X-ray Diffraction Facility, EPIC facility, Keck-II facility, and SPID facility of the NUANCE Center at Northwestern U., which received support from the Soft and Hybrid Nanotechnology Experimental (SHyNE) Resource (NSF NNCI-1542205); the MRSEC program (NSF DMR-1121262) at the Materials Research Center; the International Institute for Nanotechnology (IIN); the Keck Foundation; and the State of Illinois, through the IIN. B.W. and W.H. thank the joint-Ph.D. program supported by China Scholarship Council for fellowships.

REFERENCES

(1) Zheng, H.; Zheng, Y.; Liu, N.; Ai, N.; Wang, Q.; Wu, S.; Zhou, J.; Hu, D.; Yu, S.; Han, S.; Xu, W.; Luo, C.; Meng, Y.; Jiang, Z.; Chen, Y.; Li, D.; Huang, F.; Wang, J.; Peng, J.; Cao, Y. *Nat. Commun.* **2013**, *4*, 1971.

(2) Kim, S.; Kwon, H. J.; Lee, S.; Shim, H.; Chun, Y.; Choi, W.; Kwack, J.; Han, D.; Song, M.; Kim, S.; Mohammadi, S.; Kee, I.; Lee, S. Y. *Adv. Mater.* **2011**, *23*, 3511.

(3) Choi, Y. S.; Yun, J. U.; Park, S. E. *J. Non-Cryst. Solids* **2016**, *431*, 2.

(4) Nomura, K.; Ohta, H.; Takagi, A.; Kamiya, T.; Hirano, M.; Hosono, H. *Nature* **2004**, *432*, 488.

(5) Sirringhaus, H. *Adv. Mater.* **2014**, *26*, 1319.

(6) Thomas, S. R.; Pattanasattayavong, P.; Anthopoulos, T. D. *Chem. Soc. Rev.* **2013**, *42*, 6910.

(7) Socratous, J.; Banger, K. K.; Vaynzof, Y.; Sadhanala, A.; Brown, A. D.; Sepe, A.; Steiner, U.; Sirringhaus, H. *Adv. Funct. Mater.* **2015**, *25*, 1873.

(8) Wager, J. F.; Yeh, B.; Hoffman, R. L.; Keszler, D. A. *Curr. Opin. Solid State Mater. Sci.* **2014**, *18*, 53.

(9) Park, J. S.; Maeng, W. J.; Kim, H. S.; Park, J. S. *Thin Solid Films* **2012**, *520*, 1679.

(10) Smith, J.; Zhang, W. M.; Sougrat, R.; Zhao, K.; Li, R. P.; Cha, D. K.; Amassian, A.; Heeney, M.; McCulloch, I.; Anthopoulos, T. D. *Adv. Mater.* **2012**, *24*, 2441.

(11) Venkateshvaran, D.; Nikolka, M.; Sadhanala, A.; Lemaur, V.; Zelazny, M.; Kepa, M.; Hurhangee, M.; Kronemeijer, A. J.; Pecunia, V.; Nasrallah, I.; Romanov, I.; Broch, K.; McCulloch, I.; Emin, D.; Olivier, Y.; Cornil, J.; Beljonne, D.; Sirringhaus, H. *Nature* **2014**, *515*, 384.

(12) Ma, H.; Acton, O.; Hutchins, D. O.; Cernetic, N.; Jen, A. K. Y. *Phys. Chem. Chem. Phys.* **2012**, *14*, 14110.

(13) Mativenga, M.; Geng, D.; Jang, J. *Dig. Tech. Pap. - Soc. Inf. Disp. Int. Symp.* **2014**, *45*, 1.

(14) Xu, H.; Luo, D. X.; Li, M.; Xu, M.; Zou, J. H.; Tao, H.; Lan, L. F.; Wang, L.; Peng, J. B.; Cao, Y. *J. Mater. Chem. C* **2014**, *2*, 1255.

(15) Nakamura, T.; Tada, M.; Kimura, H. *J. Soc. Inf. Disp.* **2015**, *23*, 580.

(16) Mo, Y. G.; Kim, M.; Kang, C. K.; Jeong, J. H.; Park, Y. S.; Choi, C. G.; Kim, H. D.; Kim, S. S. *J. Soc. Inf. Disp.* **2011**, *19*, 16.

(17) Cho, D. H.; Yang, S.; Park, S. H. K.; Byun, C.; Yoon, S. M.; Lee, J. I.; Hwang, C. S.; Chu, H. Y.; Cho, K. I. *Dig. Tech. Pap. - Soc. Inf. Disp. Int. Symp.* **2009**, *40*, 280.

(18) Yang, S.; Bak, J. Y.; Yoon, S. M.; Ryu, M. K.; Oh, H.; Hwang, C. S.; Kim, G. H.; Park, S. H. K.; Jang, J. *IEEE Electron Device Lett.* **2011**, *32*, 1692.

(19) Yu, X.; Marks, T. J.; Facchetti, A. *Nat. Mater.* **2016**, *15*, 383.

(20) Zhu, H.; Liu, A.; Shan, F.; Yang, W.; Zhang, W.; Li, D.; Liu, J. *Carbon* **2016**, *100*, 201.

(21) Lin, Y. H.; Faber, H.; Zhao, K.; Wang, Q. X.; Amassian, A.; McLachlan, M.; Anthopoulos, T. D. *Adv. Mater.* **2013**, *25*, 4340.

(22) Meyers, S. T.; Anderson, J. T.; Hung, C. M.; Thompson, J.; Wager, J. F.; Keszler, D. A. *J. Am. Chem. Soc.* **2008**, *130*, 17603.

(23) Jeong, J. K. *Semicond. Sci. Technol.* **2011**, *26*, 034008.

(24) Jang, J. T.; Park, J.; Ahn, B. D.; Kim, D. M.; Choi, S. J.; Kim, H. S.; Kim, D. H. *Appl. Phys. Lett.* **2015**, *106*, 123505.

(25) Kumomi, H.; Kamiya, T.; Hosono, H. *ECS Trans.* **2015**, *67*, 3.

(26) Yu, X.; Zeng, L.; Zhou, N.; Guo, P.; Shi, F.; Buchholz, D. B.; Ma, Q.; Yu, J.; Dravid, V. P.; Chang, R. P.; Bedzyk, M.; Marks, T. J.; Facchetti, A. *Adv. Mater.* **2015**, *27*, 2390.

(27) Banger, K. K.; Yamashita, Y.; Mori, K.; Peterson, R. L.; Leedham, T.; Rickard, J.; Sirringhaus, H. *Nat. Mater.* **2011**, *10*, 45.

(28) Lee, W. J.; Park, W. T.; Park, S.; Sung, S.; Noh, Y. Y.; Yoon, M. H. *Adv. Mater.* **2015**, *27*, 5043.

(29) Park, W. T.; Son, I.; Park, H. W.; Chung, K. B.; Xu, Y.; Lee, T.; Noh, Y. Y. *ACS Appl. Mater. Interfaces* **2015**, *7*, 13289.

(30) Nadarajah, A.; Wu, M. Z. B.; Archila, K.; Kast, M. G.; Smith, A. M.; Chiang, T. H.; Keszler, D. A.; Wager, J. F.; Boettcher, S. W. *Chem. Mater.* **2015**, *27*, 5587.

(31) Rim, Y. S.; Jeong, W. H.; Kim, D. L.; Lim, H. S.; Kim, K. M.; Kim, H. J. *J. Mater. Chem.* **2012**, *22*, 12491.

(32) Kim, Y. H.; Heo, J. S.; Kim, T. H.; Park, S.; Yoon, M. H.; Kim, J.; Oh, M. S.; Yi, G. R.; Noh, Y. Y.; Park, S. K. *Nature* **2012**, *489*, 128.

(33) Kim, M. G.; Kanatzidis, M. G.; Facchetti, A.; Marks, T. J. *Nat. Mater.* **2011**, *10*, 382.

(34) Yu, X.; Smith, J.; Zhou, N. J.; Zeng, L.; Guo, P. J.; Xia, Y.; Alvarez, A.; Aghion, S.; Lin, H.; Yu, J. S.; Chang, R. P. H.; Bedzyk, M. J.; Ferragut, R.; Marks, T. J.; Facchetti, A. *Proc. Natl. Acad. Sci. U. S. A.* **2015**, *112*, 3217.

(35) Hennek, J. W.; Smith, J.; Yan, A.; Kim, M. G.; Zhao, W.; Dravid, V. P.; Facchetti, A.; Marks, T. J. *J. Am. Chem. Soc.* **2013**, *135*, 10729.

DOI: 10.1021/jacs.6b02309
J. Am. Chem. Soc. 2016, 138, 7067−7074

(36) Wang, B.; Yu, X.; Guo, P.; Huang, W.; Zeng, L.; Zhou, N.; Chi, L.; Bedzyk, M. J.; Chang, R. P. H.; Marks, T. J.; Facchetti, A. *Adv. Electron. Mater.* **2016**, *2*, 1500427.
(37) Bae, E. J.; Kang, Y. H.; Han, M.; Lee, C.; Cho, S. Y. *J. Mater. Chem. C* **2014**, *2*, 5695.
(38) Kang, Y. H.; Jeong, S.; Ko, J. M.; Lee, J. Y.; Choi, Y.; Lee, C.; Cho, S. Y. *J. Mater. Chem. C* **2014**, *2*, 4247.
(39) Jung, J. W.; Chueh, C. C.; Jen, A. K. *Adv. Mater.* **2015**, *27*, 7874.
(40) Bai, S.; Cao, M.; Jin, Y.; Dai, X.; Liang, X.; Ye, Z.; Li, M.; Cheng, J.; Xiao, X.; Wu, Z.; Xia, Z.; Sun, B.; Wang, E.; Mo, Y.; Gao, F.; Zhang, F. *Adv. Energy Mater.* **2014**, *4*, 1301460.
(41) Kim, J. H.; Liang, P. W.; Williams, S. T.; Cho, N.; Chueh, C. C.; Glaz, M. S.; Ginger, D. S.; Jen, A. K. Y. *Adv. Mater.* **2015**, *27*, 695.
(42) Kim, M. G.; Hennek, J. W.; Kim, H. S.; Kanatzidis, M. G.; Facchetti, A.; Marks, T. J. *J. Am. Chem. Soc.* **2012**, *134*, 11583.
(43) Yu, X. G.; Zhou, N. J.; Smith, J.; Lin, H.; Stallings, K.; Yu, J. S.; Marks, T. J.; Facchetti, A. *ACS Appl. Mater. Interfaces* **2013**, *5*, 7983.
(44) Hennek, J. W.; Kim, M. G.; Kanatzidis, M. G.; Facchetti, A.; Marks, T. J. *J. Am. Chem. Soc.* **2012**, *134*, 9593.
(45) Curl, R. L. *J. Am. Chem. Soc.* **1984**, *106*, 830.
(46) Marrocchi, A.; Facchetti, A.; Lanari, D.; Petrucci, C.; Vaccaro, L. *Energy Environ. Sci.* **2016**, *9*, 763.
(47) Mei, X.; Yang, H.; Li, X.; Li, Y.; Cheng, Y. *J. Therm. Anal. Calorim.* **2015**, *120*, 1749.
(48) Goll, J. G.; Wilkinson, L. J.; Snell, D. M. *J. Chem. Educ.* **2009**, *86*, 177.
(49) Klauk, H. *Chem. Soc. Rev.* **2010**, *39*, 2643.
(50) Lin, Y.-H.; Faber, H.; Labram, J. G.; Stratakis, E.; Sygellou, L.; Kymakis, E.; Hastas, N. A.; Li, R.; Zhao, K.; Amassian, A.; Treat, N. D.; McLachlan, M.; Anthopoulos, T. D. *Adv. Sci.* **2015**, *2*, 1500058.
(51) Cernetic, N.; Wu, S. F.; Davies, J. A.; Krueger, B. W.; Hutchins, D. O.; Xu, X. D.; Ma, H.; Jen, A. K. Y. *Adv. Funct. Mater.* **2014**, *24*, 3464.
(52) Kuznetsov, D. M.; Tumanov, V. V.; Smit, W. A. *J. Polym. Res.* **2013**, *20*, 128.
(53) Grimm, A.; Seubert, A. *Microchim. Acta* **2004**, *146*, 97.
(54) Oxley, J. C.; Smith, J. L.; Donnelly, M.; Porter, M. *J. Therm. Anal. Calorim.* **2015**, *121*, 743.
(55) Jeong, J. K.; Chung, H. J.; Mo, Y. G.; Kim, H. D. *J. Electrochem. Soc.* **2008**, *155*, H873.
(56) The specific per mass combustion enthalpy for sorbitol and sucrose is 16.5 kJ g^{-1}, and for glucose is 15.4 kJ g^{-1}. See: Metzler, D. E. *Biochemistry: The Chemical Reactions Of Living Cells*, 2nd ed.; Elsevier: Amsterdam, 2003; Vol. *1*. Note also that the three prinstine sugars have different decomposition temperatures (~290 °C for sorbitol, ~410 °C for glucose, and >440 °C for sucrose). Therefore, because of the complexity of the combustion reaction and the uncertain identity of all reactants and prodcuts, relating the combustion enthalpies to specific sugars and the resulting IGZO properites is premature. Additional mechanics studies will be necessary.
(57) Choi, S. H.; Han, M. K. *Appl. Phys. Lett.* **2012**, *100*, 043503.
(58) Smith, J.; Zeng, L.; Khanal, R.; Stallings, K.; Facchetti, A.; Medvedeva, J. E.; Bedzyk, M. J.; Marks, T. J. *Adv. Electron. Mater.* **2015**, *1*, 1500146.
(59) Nomura, K.; Kamiya, T.; Ohta, H.; Uruga, T.; Hirano, M.; Hosono, H. *Phys. Rev. B: Condens. Matter Mater. Phys.* **2007**, *75*, 035212.
(60) Noh, H. K.; Chang, K. J.; Ryu, B.; Lee, W. J. *Phys. Rev. B: Condens. Matter Mater. Phys.* **2011**, *84*, 115205.

■ NOTE ADDED AFTER ASAP PUBLICATION

The abstract graphic and Figure 1 have been updated and the revised version was posted on May 27, 2016.

DOI: 10.1021/jacs.6b02309
J. Am. Chem. Soc. 2016, 138, 7067−7074